

# A minimal two-band model for the superconducting Fe-pnictides

S. Raghu<sup>1</sup>, Xiao-Liang Qi<sup>1</sup>, Chao-Xing Liu<sup>2,1</sup>, D.J. Scalapino<sup>3</sup> and Shou-Cheng Zhang<sup>1</sup>

<sup>1</sup>*Department of Physics, McCullough Building, Stanford University, Stanford, CA 94305-4045*

<sup>2</sup>*Center for Advanced Study, Tsinghua University, Beijing, 100084, R. P. China and*

<sup>3</sup>*Department of Physics, University of California, Santa Barbara, CA 93106-9530*

(Dated: October 22, 2018)

Following the discovery of the Fe-pnictide superconductors, LDA band structure calculations showed that the dominant contributions to the spectral weight near the Fermi energy came from the Fe 3d orbitals. The Fermi surface is characterized by two hole surfaces around the  $\Gamma$  point and two electron surfaces around the M point of the 2 Fe/cell Brillouin zone. Here, we describe a 2-band model that reproduces the topology of the LDA Fermi surface and exhibits both ferromagnetic and  $q = (\pi, 0)$  spin density wave (SDW) fluctuations. We argue that this minimal model contains the essential low energy physics of these materials.

PACS numbers: 71.10.Fd, 71.18.+y, 71.20.-b, 74.20.-z, 74.20.Mn, 74.25.Ha, 75.30.Fv

*Introduction* - The recent discovery of superconductivity in a family of Fe-based oxypnictides with large transition temperatures [1, 2, 3, 4, 5, 6] has led to tremendous activity aimed at identifying the mechanism for superconductivity in these materials. Preliminary experimental results including specific heat [7], point-contact spectroscopy [8] and high-field resistivity [9, 10] measurements suggest the existence of unconventional superconductivity in these materials. Furthermore, transport[11] and neutron scattering[12] measurements have shown the evidence of magnetic order below  $T = 150K$ . An experimental determination of the orbital and spin state of the Cooper pairs, however, has not yet been made.

The high transition temperatures and the electronic structure of the Fe-pnictide superconductors suggest that the pairing interaction is of electronic origin.[13] First-principle band structure calculations [14, 15, 16, 17] have shown that superconductivity in these materials is associated with the Fe-pnictide layer, and that the density of states (DOS) near the Fermi level gets its maximum contribution from the Fe-3d orbitals. The consensus based on these calculations is that the Fermi surface consists of two hole pockets and two electron pockets. Calculations from Ref. [15] also show van Hove singularities which might be responsible for enhanced ferromagnetic fluctuations. The bare magnetic spin susceptibility determined from these bands exhibits both ferromagnetic  $q \sim 0$  and finite  $q$  SDW peaks.

Several tight binding models for the band structure have been proposed. Cao et al. [18] used 16 localized Wannier functions to construct a tight-binding effective Hamiltonian. Kuroki et al. [19] have used a 5 orbital tight binding model to fit the band structure near the Fermi energy. Others have introduced generic 2-band models [20, 21, 22]. However, the relationship of these latter models to the multiple Fermi surface electron and hole pockets found in LDA calculations is unclear. Since it appears likely that these multiple Fermi surfaces play an essential role in determining the momentum depen-

dence of the spin and orbital fluctuations which would mediate an electronic pairing mechanism, we would like to construct a minimal model that exhibits a Fermi surface similar to that obtained from band structure calculations.

This model has two orbitals per site on a two dimensional square lattice. By adjusting the one-electron hopping parameters and the chemical potential one can obtain a Fermi surface which has the same topology as found from the band structure calculations. The non-interacting spin susceptibility also exhibits both ferromagnetic and finite  $q$  SDW peaks. With the addition of an onsite intra-orbital and inter-orbital Coulomb interactions, and an intra-orbital Hund's rule coupling, this model represents what we believe is a minimal model for describing the low energy physics of these materials. In addition, the relative simplicity of this model should be useful in the phenomenological analysis of experiments related to the gap symmetry [23] and in numerical density-matrix renormalization group (DMRG) and dynamic cluster studies.

*Model Hamiltonian* - The structure of the FeAs layer of LaOFeAs viewed along the  $c$ -axis is illustrated in Fig. 1a. The Fe ions form a square lattice which is interlaced with a second square lattice of As ions. These As ions sit in the center of each square plaquette of the Fe lattice and are displaced above and below the plane of the Fe ions as indicated in the figure. This leads to two distinct Fe sites and a crystallographic unit cell which contains two Fe and two As ions. As shown by various band structure calculations, the main contribution to the density of states within several eV of the Fermi surface comes from the Fe 3d states which disperse only weakly in the  $z$ -direction. The 3d Fe orbitals hybridize among themselves and through the As  $p$  orbitals leading to a complex of bands. However, as noted in Ref. [16], the bandstructure near the Fermi level is relatively simple in the unfolded 1Fe/cell BZ where it primarily involves three Fe orbitals  $d_{xz}$ ,  $d_{yz}$  and  $d_{xy}$  (or  $d_{x^2-y^2}$ ). Based upon this

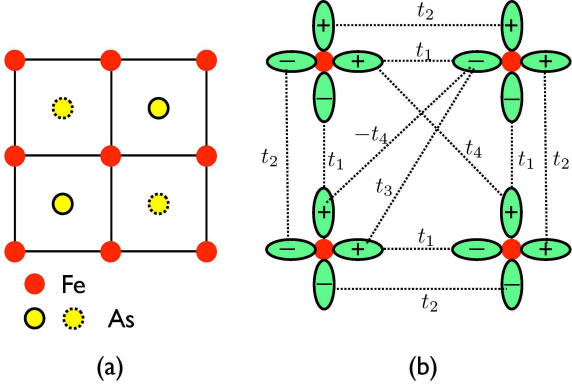


FIG. 1: (a) The Fe ions form a square lattice and the crystallographic unit cell contains two Fe and two As ions. The As ions are located either directly above (solid circles) or below (dashed circles) the faces of the Fe square array. (b) A schematic showing the hopping parameters of the two-orbital  $d_{xz} - d_{yz}$  model on a square lattice. Here  $t_1$  is a near neighbor hopping between  $\sigma$ -orbitals and  $t_2$  is a near neighbor hopping between  $\pi$ -orbitals. We also include a second-neighbor hopping  $t_4$  between different orbitals and a second-neighbor hopping  $t_3$  between similar orbits.

observation and by making the further approximation that the role of the  $d_{xy}$  ( $d_{x^2-y^2}$ ) orbit can be replaced by a next near neighbor hybridization between  $d_{xz}$ ,  $d_{zy}$  orbitals, we consider a two-dimensional square lattice with two degenerate “ $d_{xz}$ ,  $d_{yz}$ ” orbitals per site. While one may well need a third orbit to control the relative sizes and eccentricities of the electron and hole pockets, we find that a two-orbital model can lead to a Fermi surface which resembles that obtained in the bandstructure calculations.

The tight-binding parameters of the 2-orbital model that we will study are illustrated in Fig. 1. It is convenient to introduce a two-component field

$$\psi_{ks} = \begin{pmatrix} d_{xs}(k) \\ d_{ys}(k) \end{pmatrix} \quad (1)$$

Here  $d_{xs}(k)$  ( $d_{ys}(k)$ ) destroys a  $d_{xz}$  ( $d_{yz}$ ) electron with spin  $s$  and wave vector  $k$ . Then the tight binding part of the Hamiltonian can be written as

$$H_0 = \sum_{ks} \psi_{ks}^\dagger [(\epsilon_+(k) - \mu) 1 + \epsilon_-(k)\tau_3 + \epsilon_{xy}(k)\tau_1] \psi_{ks}, \quad (2)$$

with  $\tau_i$  the Pauli matrices and

$$\begin{aligned} \epsilon_\pm(k) &= \frac{\epsilon_x(k) \pm \epsilon_y(k)}{2}, \\ \epsilon_x(k) &= -2t_1 \cos k_x - 2t_2 \cos k_y - 4t_3 \cos k_x \cos k_y, \\ \epsilon_y(k) &= -2t_2 \cos k_x - 2t_1 \cos k_y - 4t_3 \cos k_x \cos k_y, \\ \epsilon_{xy}(k) &= -4t_4 \sin k_x \sin k_y. \end{aligned}$$

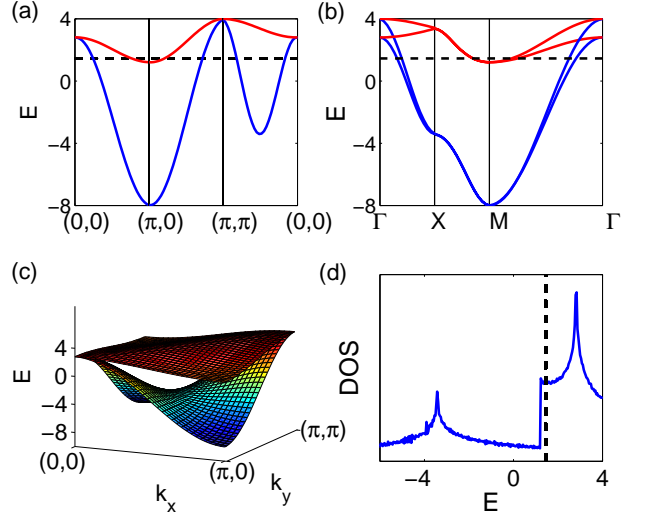


FIG. 2: (a) The band structure of the two-band model with  $t_1 = -1$ ,  $t_2 = 1.3$ ,  $t_3 = t_4 = -0.85$  and  $\mu = 1.45$ , plotted along the path  $(0,0) \rightarrow (\pi,0) \rightarrow (\pi,\pi) \rightarrow (0,0)$  as shown in Fig. 3 (a) by the black dashed lines. (b) The band structure folded to the small BZ, with the  $\Gamma, X, M$  defined in the small BZ as shown in Fig. 3 (b). (c) The two-d band structure for  $k_x, k_y \in [0, \pi]$ . A saddle point exists for each band. (d) The density of states of the two band model, with two Van Hove singularities. The dashed line shows the fermi level corresponding to our choice of  $\mu = 1.45$ .

The one electron Matsubara Green’s function is given by

$$\hat{G}_s(\mathbf{k}, i\omega_n) = \frac{(i\omega_n - \epsilon_+(\mathbf{k})) \hat{1} - \epsilon_-(\mathbf{k})\hat{\tau}_3 - \epsilon_{xy}(\mathbf{k})\hat{\tau}_1}{(i\omega_n - E_+(\mathbf{k}))(i\omega_n - E_-(\mathbf{k}))} \quad (3)$$

with

$$E_\pm(\mathbf{k}) = \epsilon_+(\mathbf{k}) \pm \sqrt{\epsilon_x^2(\mathbf{k}) + \epsilon_y^2(\mathbf{k})} - \mu \quad (4)$$

In Figure 2 we show the band structure of the model for a specific choice of hopping parameters  $t_1 = -1$ ,  $t_2 = 1.3$ ,  $t_3 = t_4 = -0.85$ , in units of  $|t_1|$ . The folded energy spectrum in Fig. 2 (b) shows the band structure in the 2 Fe/cell zone. Due to the saddle points in the energy spectrum (as shown in Fig. 2 (c)), there are two Van Hove singularities in the density of states, which also qualitatively agrees with the LDA results.[15] In Figure 3 we show the Fermi surface for the same set of parameters. On the large BZ (Fig. 3a) associated with our model which has 1 Fe/unit cell, there are two hole Fermi pockets labeled  $\alpha_1$  and  $\alpha_2$  defined by  $E_-(\mathbf{k}) = 0$ , and two electron Fermi pockets  $\beta_1$  and  $\beta_2$  defined by  $E_+(\mathbf{k}) = 0$ . To compare with band structure calculations, one must fold the large BZ into a smaller one which is dual to the crystallographic unit cell containing two Fe atoms. The dashed square in Fig. 3 (a) marks this smaller zone and in Fig. 3 (b) we show what happens as the  $\alpha_{1,2}$  and  $\beta_{1,2}$

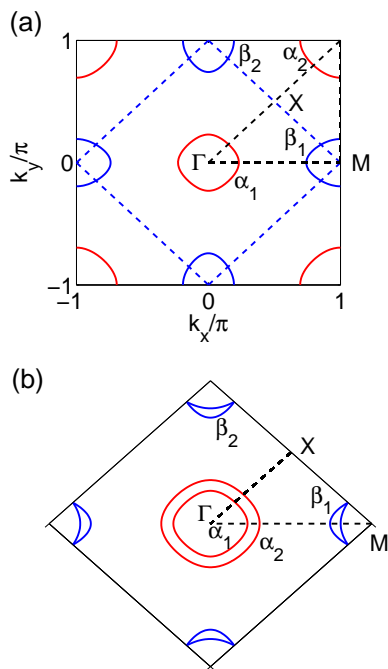


FIG. 3: (a) The Fermi surface of the 2-orbital model on the large 1Fe/cell BZ. Here,  $\alpha_{1,2}$  surfaces are hole Fermi pockets given by  $E_-(\mathbf{k}_f) = 0$  and  $\beta_{1,2}$  are electron Fermi pockets by  $E_+(\mathbf{k}_f) = 0$ . The dashed square indicates the BZ of the 2Fe/cell. (b) The Fermi surface folded down into the 2 Fe/cell BZ consists of two  $\alpha$  surfaces around  $\Gamma$  and two elliptically deformed  $\beta$  surfaces around the  $M$  point. Here the parameters are the same as in Fig. 2

bands of Fig. 3 (a) are folded back into the 2Fe/cell BZ. One sees that this gives Fermi surfaces with the same topology that is obtained from LDA band structure calculations [24].

*One-loop spin susceptibility.*— Now we study the one-loop spin-susceptibility for the tight-binding model (2). Due to the existence of two degenerate orbitals in our model, the spin susceptibility also has orbital indices, and is defined by

$$\chi_{st}(\mathbf{q}, i\Omega) = \int_0^\beta d\tau e^{i\Omega\tau} \langle T_\tau \mathbf{S}_s(-\mathbf{q}, \tau) \cdot \mathbf{S}_t(\mathbf{q}, 0) \rangle \quad (5)$$

here  $s, t = 1, 2$  label the orbital indices, and  $\mathbf{S}_s(\mathbf{q}) = \frac{1}{2} \sum_{\mathbf{k}} \psi_{s\alpha}^\dagger(\mathbf{k} + \mathbf{q}) \vec{\sigma}_{\alpha\beta} \psi_{s\beta}(\mathbf{k})$  is the spin operator for the orbital labeled by  $s$ . The physical spin susceptibility is given by

$$\chi_S(\mathbf{q}, i\Omega) = \sum_{s,t} \chi_{st}(\mathbf{q}, i\Omega).$$

The one loop contribution to the spin susceptibility can

be obtained as

$$\begin{aligned} \chi_S(\mathbf{q}, i\Omega) &= -\frac{T}{2N} \sum_{\mathbf{k}, \omega_n} \text{Tr} [G(\mathbf{k} + \mathbf{q}, i\omega_n + i\Omega) G(\mathbf{k}, i\omega_n)] \\ &= -\frac{1}{2N} \sum_{\mathbf{k}, \nu, \nu'} \frac{|\langle \mathbf{k} + \mathbf{q}, \nu | \mathbf{k}, \nu' \rangle|^2}{i\Omega + E_{\nu, \mathbf{k} + \mathbf{q}} - E_{\nu', \mathbf{k}}} \\ &\quad \cdot (n_F(E_{\nu, \mathbf{k} + \mathbf{q}}) - n_F(E_{\nu', \mathbf{k}})) \end{aligned} \quad (6)$$

Here  $E_{\nu \mathbf{k}}$ ,  $\nu = +1(-1)$  is the eigenvalue of the upper (lower) band given by Eq. (4), and  $|\mathbf{k}, \nu\rangle$  the corresponding eigenvector.  $n_F(E) = 1/(e^{\beta E} + 1)$  is the fermi distribution function.

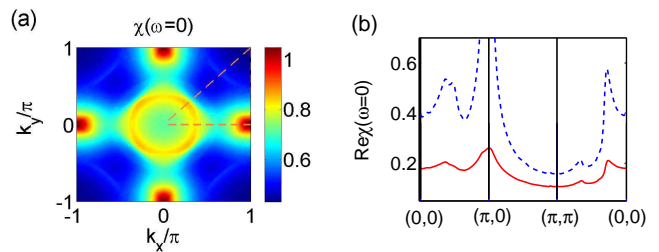


FIG. 4: (a) The  $\omega = 0$  bare spin susceptibility  $\chi_S(\mathbf{q})$  versus  $\mathbf{q}$  for the same tight-binding parameters as used in Fig. 3. (b) The bare spin susceptibility  $\chi_S(\mathbf{q})$  (red solid line) and the RPA spin susceptibility  $\chi_S^{\text{RPA}}(\mathbf{q})$  for  $U = V = 6$ ,  $J = 0$  (blue dashed line) along the  $(0,0) \rightarrow (\pi,0) \rightarrow (\pi,\pi) \rightarrow (0,0)$  path in BZ, as shown by the dashed line in subfigure (a).

Fig. 4 shows a plot of the static spin susceptibility  $\chi_S(q, 0)$  versus  $q$ , where one can see the structure associated with the various nesting points and density of states features. For our choice of parameters, the largest value of  $\chi_0(q)$  occurs around  $q = (\pi, 0)$  and  $(0, \pi)$ , which suggests a transition to an antiferromagnetic (AFM) ordered phase at some critical interaction strength. This is also in agreement with the result of band structure calculations[16, 25]. A recent neutron scattering experiment has confirmed that such a peak develops below  $T \sim 150K$  [12]. Such a peak in the spin susceptibility comes from the nesting between the electron and hole Fermi pockets, which can be seen from the chemical potential dependence of the spin susceptibility. As shown in Fig. 5, the spin susceptibility at  $q = (0, 0)$  jumps discontinuously at  $\mu \sim 1.2$ , which follows the behavior of the density of states shown in Fig. 2 (d), and corresponds to the onset of electron Fermi pockets. At the same time, the  $q = (0, \pi)$  spin susceptibility is also enhanced significantly due to the nesting effect. When the chemical potential is increased further, the fermi level gets closer to the Van Hove singularity, and the hot point of the spin susceptibility is shifted gradually to the neighborhood of  $(0, 0)$  and  $(\pi, \pi)$ , as shown in Fig. 5 (b).

*The RPA spin susceptibility.*— Now we consider the effect of electron-electron interaction in this model. For the two  $d$  orbitals we considered, the generic form of the

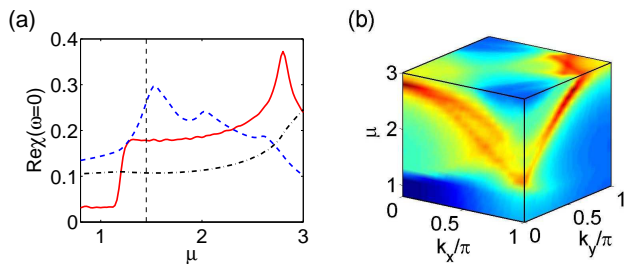


FIG. 5: (a) The chemical potential dependence of  $\text{Re}\chi(\mathbf{q}, \omega = 0)$  with  $\mathbf{q} = (0, 0)$ ,  $(0, \pi)$  and  $(\pi, \pi)$ . The vertical dashed line shows the chemical potential  $\mu = 1.45$  which we are working on. (b) The three-d color plot of spin susceptibility as a function of  $k_x, k_y$  and chemical potential  $\mu$ . The hot points in BZ shifts from  $(\pi, 0)$  to  $(0, 0)$  and  $(\pi, \pi)$  with electron doping as  $\mu$  increases. The deepest red region shows the Van Hove singularities.

on-site interaction can be written as

$$H_{\text{int}} = \sum_i \left( U \sum_s n_{is\uparrow} n_{is\downarrow} + V n_{i1} n_{i2} - J \mathbf{S}_{i1} \cdot \mathbf{S}_{i2} \right) \quad (7)$$

with  $U$  and  $V$  the intraband and interband Coulomb repulsion, and  $J$  the Hunds rule coupling. For an isolated Fe atom, the intraband  $U$  and interband  $V$  are similar in magnitude, and  $J$  is an order of magnitude smaller [26]. Thus we expect the  $U$  and  $V$  to be the dominant terms in the interaction. We suggest that  $H = H_0 + H_{\text{int}}$  represents a minimal model for the Fe-pnictides superconductors.

Next we will study the effect of such interactions on the spin fluctuations within RPA. Due to the two band nature of the model we considered, the RPA correction should be calculated for the generic spin susceptibility  $\chi_{st}(\mathbf{q}, i\Omega)$  defined in Eq. (5), which is determined by the following matrix equation:

$$\chi^{\text{RPA}}(\mathbf{q}, i\Omega) = \chi_0(\mathbf{q}, i\Omega) (\mathbb{I} - \Gamma \chi_0(\mathbf{q}, i\Omega))^{-1} \quad (8)$$

Here  $\chi_0$  is the  $2 \times 2$  matrix formed by the intra-orbital and inter-orbital spin susceptibility defined in Eq. (5), and  $\Gamma$  is the interaction vertex defined by

$$\Gamma = \begin{pmatrix} U & J/2 \\ J/2 & U \end{pmatrix} \quad (9)$$

We note that the interband interaction  $V$  does not contribute to the RPA response when only the spin fluctuations are considered.

In the following we set  $J = 0$ , which makes the interaction vertex  $\Gamma$  in Eq. (9) proportional to the identity. For the tight-binding model parameters used in Fig. 3 and  $U = 6$ , we obtain the RPA spin susceptibility shown in Fig. 4 (b) by the dashed line. As expected, the spin susceptibility is enhanced around the hot points  $(\pi, 0)$  and  $(0, \pi)$ . We have also carried out the RPA calculation

for a finite Hunds rule coupling  $J > 0$ , and find that the spin fluctuations are enhanced by increasing  $J$ , but the structure of  $\chi(\mathbf{q})$  remains qualitatively the same.

In conclusion, we have described a minimal model for the Fe-pnictides which we believe contains the essential low energy physics of these materials. This model consists of a two dimensional square lattice of sites with each site having two degenerate orbitals. By fitting the tight binding parameters, one can obtain a band structure which, after folded to the  $2\text{Fe}/\text{cell}$  BZ, exhibits two hole pockets around the  $\Gamma$  point and two electron pockets around the  $M$  point. The electron-electron interactions are taken to be onsite intra-orbital and inter-orbital Coulomb interactions  $U$  and  $V$  and an onsite Hund's rule coupling  $J$ . The structure of the bare spin susceptibility is peaked around  $(\pi, 0)$  for the parameters we chose to fit the fermi surface. Such AFM spin fluctuations also leads to the possibility of non-conventional superconductivity, which we will discuss in a separate work. Different types of spin or orbital orders and superconductivity can possibly occur for different fillings. Therefore, we conclude that this model contains a rich variety of magnetic, orbital and pairing correlations.

We would like to acknowledge X. Dai, Z. Fang and H. J. Zhang for many insightful discussions and for generous sharing of their unpublished work. We acknowledge helpful discussions with S. Kivelson, R. Martin, I. Mazin, T. Schulthess, D. Singh and H. Yao. We would also like to thank the authors of Ref. [23] for sending us their paper prior to submission. This work is supported by the NSF under grant numbers DMR-0342832, the US Department of Energy, Office of Basic Energy Sciences under contract DE-AC03-76SF00515, the center for nanophase material science, ORNL (DJS) and the Stanford Institute for Theoretical Physics (SR, DJS).

- 
- [1] Y. Kamihara, T. Watanabe, M. Hirano, and H. Hosono, *J. Am. Chem. Soc.* **130**, 3296 (2008).
  - [2] Z.-A. Ren, J. Yang, W. Lu, G.-C. Che, X.-L. Dong, L.-L. Sun, and Z.-X. Zhao, e-print arxiv: 0803.4283 (2008).
  - [3] G. Chen, Z. Li, G. Li, J. Zhou, D. Wu, W. Hu, P. Zheng, Z. Chen, J. Luo, and N. Wang, e-print arxiv: 0803.0128 (2008).
  - [4] X. Chen, T. Wu, G. Wu, R. Liu, H. Chen, and D. Fang, e-print arxiv: 0803.3603 (2008).
  - [5] G. Chen, Z. Li, D. Wu, G. Li, W. Z. Hu, J. Dong, P. Zheng, J. Luo, and N. Wang, e-print arxiv: 0803.3790 (2008).
  - [6] H.-H. Wen, G. Mu, L. Fang, H. Yang, and X. Zhu, *Europhys. Lett.* **82**, 17009 (2008).
  - [7] G. Mu, X. Zhu, L. Fang, L. Shan, C. Ren, and H.-H. Wen, e-print arxiv: 0803.0928 (2008).
  - [8] L. Shan, Y. Wang, X. Zhu, G. Mu, L. Fang, and H.-H. Wen, e-print arxiv: 0803.2405 (2008).
  - [9] F. Hunte, J. Jaroszynski, A. Gurevich, D. Larbalestier,

- R. Jin, A. Sefat, M. McGuire, B. Sales, D. Christen, and D. Mandrus, e-print arxiv: 0804.0485 (2008).
- [10] X. Zhu, H. Yang, L. Fang, G. Mu, and H.-H. Wen, e-print arxiv: 0803.1288 (2008).
- [11] J. Dong, H. J. Zhang, G. Xu, Z. Li, G. Li, W. Z. Hu, D. Wu, G. F. Chen, X. Dai, J. L. Luo, et al., e-print arxiv:0803.3426 (2008).
- [12] C. de la Cruz, Q. Huang, J. W. Lynn, J. Li, W. R. II, J. L. Zarestky, H. A. Mook, G. F. Chen, J. L. Luo, N. L. Wang, et al., e-print arxiv: 0804.0795 (2008).
- [13] L. Boeri, O. Dolgov, and A. Golubov, e-print arxiv: 0803.2703 (2008).
- [14] D. Singh and M.-H. Du, e-print arxiv: 0803.0429 (2008).
- [15] G. Xu, W. Ming, Y. Yao, X. Dai, S.-C. Zhang, and Z. Fang, e-print arxiv: 0803.1282 (2008).
- [16] I. Mazin, D. Singh, M. Johannes, and M.-H. Dou, e-print arxiv: 0803.2740 (2008).
- [17] K. Haule, J. H. Shim, and G. Kotliar, arxiv: 0803.1279 (2008).
- [18] C. Cao, P. J. Hirschfeld, and H.-P. Cheng, arxiv: 0803.3236 (2008).
- [19] K. Kuroki, S. Onari, R. Arita, H. Usui, Y. Tanaka, H. Kontani, and H. Aoki, e-print arxiv: 0803.3325 (2008).
- [20] X. Dai, Z. Fang, Y. Zhou, and F.-C. Zhang, e-print arxiv: 0803.3982 (2008).
- [21] Q. Han, Y. Chen, and Z. Wang, e-print arxiv: 0803.4346 (2008).
- [22] T. Li, e-print arxiv:0804.0536 (2008).
- [23] S. Graser, G. Boyd, C. Cao, H.-P. Cheng, P. J. Hirschfeld, and D. J. Scalapino, e-print arxiv: 0804.0887 (2008).
- [24] The relative size of the Fermi velocity associated with the  $\alpha$  and  $\beta$  bands is not accurate and additional orbitals or a phenomenological adjustment would be required to fit the band structure precisely.
- [25] H.-J. Zhang, G. Xu, X. Dai, and Z. Fang, e-print arxiv: 0803.4487 (2008).
- [26] I. Schnell, G. Czycholl, and R. C. Albers, Phys. Rev. B **68**, 245102 (2003).